



Comparative Study of Conventional Electrolytes for Rechargeable Magnesium Batteries

Raymond Horia^{+, [a, b]}, Dan-Thien Nguyen^{+, [a]}, Alex Yong Sheng Eng,^[a] and Zhi Wei Seh^{*[a]}

Conventional magnesium salts are generally considered to be passivating to the magnesium anode, hence chloride-based electrolyte additives are often added to circumvent this issue. As a result, the performance of conventional magnesium salts has rarely been assessed in a chloride-free system. This work provides a comparative study on the electrochemical performance and interfacial reaction of four commercially available magnesium salts with tetrabutylammonium borohydride as moisture scavenger. Magnesium bis(hexamethyldisilazide) was found to be the most reductively stable and enabled excellent

magnesium plating/stripping without chloride additive. Investigation of the solid electrolyte interphase revealed a thin organic polyether layer that was conducive to magnesium-ion migration. The results also showed that a minuscule amount of chloride (20 mM) improved the reversibility of magnesium plating/stripping but was still corrosive towards the current collector, thus establishing that chloride-free electrolyte is most appropriate for future development of rechargeable magnesium batteries.

Introduction

Rechargeable lithium-ion batteries (LIBs) are increasingly used in various personal electronic devices, electric vehicles, and grid-scale energy storage due to their high energy density, long cycle life, and cost efficiency.^[1] However, emerging battery chemistries such as magnesium (Mg)-, aluminium (Al)-, and sodium (Na)-based chemistries are being explored since these elements are much more abundant than lithium (Li).^[2] As the current lithium reserve may not be able to meet the future demands for LIBs,^[3] the development of next-generation sustainable rechargeable batteries is important. Mg metal anode also offers high theoretical volumetric capacity (3833 mAh cm⁻³ vs. 2046 mAh cm⁻³ for Li metal and 760 mAh cm⁻³ for graphite), high gravimetric capacity (2205 mAh g⁻¹), along with low reduction potential (-2.38 V vs. SHE).^[4] The major challenges in developing rechargeable magnesium batteries are to prevent internal short-circuit caused by non-homogeneous magnesium deposition,^[5] develop high-energy-density cathodes,^[6] and to create a high-performance magnesium electrolyte with a wide potential window, non-corrosiveness to the current collector, and high stability against the magnesium anode.^[7]

In recent years, the development of rechargeable magnesium battery electrolytes has achieved major milestones. The development of these electrolytes can be traced back to the chloride-based electrolytes which were known to cause corrosion on non-noble metal current collectors such as stainless steel and aluminium.^[8] Due to this issue, chloride-based electrolytes have a lower potential window on non-noble metal current collectors as compared to Pt electrode.^[9] The need to eliminate corrosion has led to the development of high-performance chloride-free electrolytes. Amongst these salts, magnesium tetrakis(hexafluoroisopropoxy)borate or Mg-[B(HFIP)₄]₂ receives the greatest attention. Mg[B(HFIP)₄]₂-based electrolytes also have a wide potential window of 4.3 V, high magnesium plating-stripping Coulombic efficiency (CE, > 98%), high ionic-conductivity (up to 11 mS cm⁻¹), and good compatibility with high capacity sulfur cathode.^[10] Unfortunately, the commercial viability of producing new magnesium salts such as Mg[B(HFIP)₄]₂ is unknown, unlike commercial magnesium salts which are readily available in the market. Moreover, several critical issues discovered in the Mg[B(HFIP)₄]₂ electrolyte, such as short-circuit formation, batch performance variability, and magnesium-induced electrolyte decomposition, also highlight the need to explore other formulations.^[11]

An alternative pathway to develop viable electrolyte formulations is to utilize conventionally available magnesium salts for the electrolyte. As conventional magnesium salts in ethereal solvents tend to be passivating towards the magnesium anode, additives are commonly used in the electrolytes to improve the reversibility of the magnesium plating and stripping process. Several additives have been previously used including I₂, GeCl₄, or SnCl₂ as artificial interface initiators,^[12] and MgCl₂, or Mg(BH₄)₂ which act as passivation inhibitors.^[8,9b,13] The commonly used chloride-based additives, unfortunately, are known to induce corrosion of non-noble metal current collectors such as aluminum or stainless steel at high potential.^[5,7a,14] Recent study showed that conventional

[a] R. Horia,⁺ Dr. D.-T. Nguyen,⁺ Dr. A. Y. S. Eng, Prof. Z. W. Seh
Institute of Materials Research and Engineering
Agency for Science, Technology and Research (A*STAR)
2 Fusionopolis Way, Innovis, Singapore 138634, Singapore
E-mail: sehwz@imre.a-star.edu.sg

[b] R. Horia⁺
School of Materials Science and Engineering
Nanyang Technological University
50 Nanyang Avenue, Singapore 639798, Singapore

[+] These authors contributed equally to this work.

 Supporting information for this article is available on the WWW under
<https://doi.org/10.1002/batt.202200011>

 An invited contribution to a Special Collection dedicated to the 5-Year Anniversary of Batteries & Supercaps

chloride-free electrolytes can achieve excellent Mg plating/stripping through solvation sheath reorganization of Mg^{2+} cation with methoxyethyl-amines,^[15] which points to the importance of conventional electrolytes for the future development of rechargeable magnesium batteries.

Up to date, however, few comparative studies have been done to study the compatibility of conventional magnesium salts against the magnesium electrode.^[16] In this study, we aim to establish a deeper understanding of the conventional electrolyte system by evaluating the compatibility of commercially available Mg salts, including magnesium trifluoromethanesulfonate $[Mg(OTf)_2]$, magnesium bis(trifluoromethanesulfonimide) $[Mg(TFSI)_2]$, magnesium bis(hexamethyldisilazide) $[Mg(HMDS)_2]$, and magnesium perchlorate $[Mg(ClO_4)_2]$ at optimized conditions. Even though the presence of moisture is well known to inhibit the reversibility of Mg plating/stripping by the formation of passivation layer, the removal of moisture impurity in conventional electrolytes has not been investigated carefully. Our recent study on $Mg(HMDS)_2$ -based electrolytes showed that the use of a small amount of moisture scavenger enables reversible Mg plating/stripping with excellent CE.^[17] Hence, to avoid the impact of moisture contamination, we introduced tetrabutylammonium borohydride ($TBABH_4$) as a moisture scavenger. The effect of chloride additive at minute concentration on the reversibility of Mg plating/stripping and corrosion of current collector is also investigated.

Results and Discussion

Compatibility of conventional electrolytes with Mg anode

In this study, we conducted galvanostatic plating and stripping using four conventional electrolytes, including $Mg(OTf)_2$, $Mg(TFSI)_2$, $Mg(HMDS)_2$, and $Mg(ClO_4)_2$ in 1,2-dimethoxyethane (DME). Figure S1A shows the images of four conventional salt-based electrolytes in DME at a concentration of 0.1 M after stirring at 40 °C for at least 12 hours. $Mg(HMDS)_2$ and $Mg(TFSI)_2$

salt are well dissolved. A thin translucent phase on the bottom of the $Mg(TFSI)_2$ in DME solution is consistent with the liquid phases separation, similar to that reported by Salama *et al.*^[18] Other salts such as $Mg(OTf)_2$ and $Mg(ClO_4)_2$ are not fully dissolved in the DME solvent with a trace amount of white powder remaining undissolved. The conductivity of the conventional salts-based electrolytes is shown in Table S1. The ionic conductivity of these DME solutions lies in the order of $Mg(TFSI)_2$ (0.198 mS cm^{-1}) $>$ $Mg(ClO_4)_2$ (0.061 mS cm^{-1}) $>$ $Mg(OTf)_2$ (0.019 mS cm^{-1}) $>$ $Mg(HMDS)_2$ (0.006 mS cm^{-1}). Despite having high solubility, the low ionic conductivity of $Mg(HMDS)_2$ is due to its low ionic dissociation. Our previous study on the $Mg(HMDS)_2$ /DME electrolyte using single-crystal X-ray diffraction (XRD) reveals the formation of $Mg(HMDS)_2(\text{DME})$ species in DME solution, which is consistent with the low ionic conductivity of $Mg(HMDS)_2$ electrolyte.^[17,19]

Figure 1(A) shows the first plating/stripping cycle in each of the conventional electrolytes with the concentration of Mg salts fixed at 0.1 M. The result shows that the magnesium deposition process at 0.05 mA cm^{-2} and 0.05 mAh cm^{-2} occurs at a high overpotential ($> 1 \text{ V}$) and is highly irreversible in all electrolyte systems tested. In particular, the $Mg(HMDS)_2$ electrolyte shows a rapid voltage drop to -3.0 V , and no stripping capacity was obtained as the cell potential reached the cut-off potential. The $Mg(ClO_4)_2$ electrolyte shows a voltage drop to -1.0 V and gradually decreased with discharge time. This suggests that electrolyte decomposition and passivation are dominant processes instead of Mg plating, supported by no magnesium stripping being observed in the reverse process. The decreasing magnesium plating potential in the $Mg(ClO_4)_2$ electrolyte with discharge time further supports the passivating effect of ClO_4^- ion. On the contrary, $Mg(TFSI)_2$ and $Mg(OTf)_2$ demonstrate a typical plating profile of conventional electrolytes with voltage delay at the beginning of Mg plating, followed by gradually increasing cell voltage. However, a small stripping capacity in both electrolytes suggested that the irreversible reduction of electrolyte and/or contaminants (i.e., moisture) are still dominant in the initial plating process. Alternatively, the magnesium dissolution potential in the first

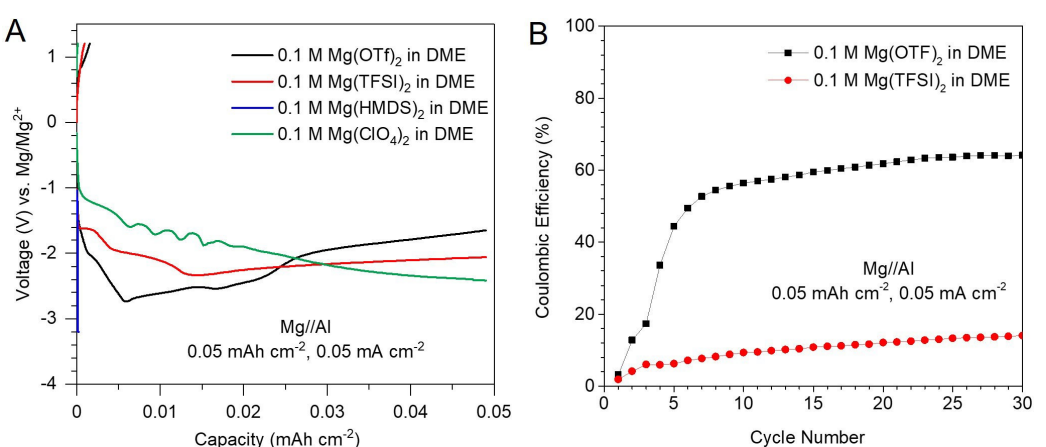


Figure 1. A) Comparison of voltage profile of first plating and stripping cycle and B) Coulombic efficiency of electrolyte solutions at 0.05 mA cm^{-2} , 0.05 mAh cm^{-2} .

cycle may be higher than the cut-off potential (1.2 V) to be observed. With increased cycle numbers (Figure 1B), only Mg(OTf)₂ and Mg(TFSI)₂ electrolyte demonstrates reversible Mg plating/stripping process with low CE of 64% and 14%, respectively. As the deposition potential of magnesium in the Mg(HMDS)₂ and Mg(ClO₄)₂ electrolytes reached below the cut-off potential of the cell cycling parameter (-3.25 V), the cells containing these electrolytes stopped cycling after at most 3 cycles. Thus, the cycling performance of these electrolytes is not shown in Figure 1(B).

Influence of electrolyte additives on electrochemical performance

The moisture and electrolyte contaminants have an undesirable impact on the performance of Mg batteries by forming a passivation layer on the surface of the Mg anode.^[9b,17,20] The reaction of Mg anode with moisture upon contacting with electrolyte leads to the formation of Mg(OH)₂, which passivates the Mg surface. Hence, to obtain an accurate picture of the influence of Mg salts on the reversibility of the Mg plating/stripping process, the moisture must be removed from the electrolyte solution before contacting with Mg metal anode. In this study, we used TBABH₄ at a very low concentration as moisture scavenger ($\text{BH}_4^- + 4\text{H}_2\text{O} \rightarrow 4\text{H}_2\uparrow + \text{B}(\text{OH})_4^-$).^[21] The TBA⁺ is used as a counterion since it is known to be reductively stable against the magnesium metal.^[22]

With the addition of 30 mM of TBABH₄ (~0.8 wt%, Table S1), we observed changes in the physical properties of electrolyte solutions (Figure S1B). First, the phase separation of 0.1 M Mg(TFSI)₂/DME solution disappears upon the addition of TBABH₄. It should be noted that the formation of two immiscible liquids observed in low concentrations of Mg(TFSI)₂ in DME is due to different DME conformer distributions.^[23] A recent publication by Chen et al. suggests that the low-density phase consists of contact-ion pair clusters with low Mg(TFSI)₂ concentration (0.06 M) while the high-density phase consists of fully dissociated Mg(TFSI)₂ with high concentration (0.36 M).^[24] The electrostatic interaction between Mg²⁺ ions in the solution was suggested to determine the stability of both phases. The addition of other salts therefore could affect the phase stability of Mg(TFSI)₂ in DME by tuning the electrostatic interaction in the solution. Additional experiment with tetrabutylammonium triflate and tetrabutylammonium chloride (Figure S2) shows a

similar result as TBABH₄, further supporting this hypothesis. Understanding the mechanism of such interaction is beyond the scope of this study.

Second, the ionic conductivity of electrolyte solution significantly increases (Table S1), especially with Mg(HMDS)₂ and Mg(OTf)₂ electrolytes. The ionic conductivity of the electrolytes are as follows: 0.74 mS cm⁻¹ for Mg(TFSI)₂, 0.42 mS cm⁻¹ for Mg(HMDS)₂, 0.21 mS cm⁻¹ for Mg(OTf)₂, and 0.12 mS cm⁻¹ for Mg(ClO₄)₂. This is related to the presence of quaternary ammonium cations (i.e., TBA⁺) in the electrolyte solution, which promotes the dissociation of Mg salts.^[22] Gofer et al. similarly observed the increase in ionic conductivity after introducing tetrabutylammonium chloride into Mg electrolyte.^[22] In the Mg(ClO₄)₂ electrolyte, the addition of TBABH₄, however, results in the formation of white precipitation, suggesting the possibility of reaction between Mg(ClO₄)₂ and TBABH₄.

Figure 2(A–C) and Table 1 shows the plating/stripping profile of Mg(TFSI)₂, Mg(OTf)₂, and Mg(HMDS)₂ in DME with 30 mM of TBABH₄ at 0.5 mAh cm⁻² and 0.5 mA cm⁻² (that of Mg(ClO₄)₂ is shown in Figure S3A). The first three electrolytes show remarkably decreased plating overpotential and increased Mg plating/stripping CE compared to that without additive (Table 1). The Mg(TFSI)₂ electrolyte, however, shows short cycle life with a huge CE drop after 3 cycles. The increased overpotential together with a low CE suggests that severe decomposition of TFSI⁻ and/or electrolyte components took place at these initial cycles and passivated the Mg electrode. Similarly, the high deposition overpotential in the Mg(ClO₄)₂/DME + 30 mM TBABH₄ (Figure S3A) electrolyte supports the previous reports on the passivation of Mg(ClO₄)₂.^[8] The asymmetric cell with Mg(OTf)₂/DME + 30 mM TBABH₄ electrolyte was able to cycle up to 40 cycles with the CE reaches to 95.7% and maintained above 80% during cycle life. However, a relatively short cycle life suggests the passivation of Mg anode remains challenging with triflate electrolyte. We believe that the passivation of the magnesium metal anode in the Mg(OTf)₂/DME + 30 mM TBABH₄ electrolyte occurs incrementally. The gradually increased overpotential of Mg plating/stripping profile (Figure 2B) supports this hypothesis. As the magnesium deposition process is repeated continuously with each cycle, the OTf⁻ decomposition reaction will continue to happen until the surface film on the anode becomes significantly thick to completely passivate the anode.

Remarkably, 0.1 M Mg(HMDS)₂/DME + 30 mM TBABH₄ shows superior cycling performance among the three electrolyte

Table 1. Summary of electrochemical performance of Mg(TFSI)₂, Mg(OTf)₂, and Mg(HMDS)₂ in DME electrolytes at 0.5 mAh cm⁻² and 0.5 mA cm⁻². The plating overpotential was determined at 50% capacity of plating profiles. Average Coulombic efficiencies were calculated over cell cycle life.

Electrolyte	Initial Coulombic efficiency [%]	Plating overpotential [V]	Highest Coulombic efficiency [%]	Average Coulombic efficiency [%]	Cycle life
0.1 M Mg(TFSI) ₂ /DME + 30 mM TBABH ₄	75.2	-0.20	75.2	17.8	23
0.1 M Mg(TFSI) ₂ /DME + 30 mM TBABH ₄ + 20 mM MgCl ₂	76.2	-0.20	77.5	21.8	29
0.1 M Mg(OTf) ₂ /DME + 30 mM TBABH ₄	95.7	-0.30	95.7	88.6	43
0.1 M Mg(OTf) ₂ /DME + 30 mM TBABH ₄ + 20 mM MgCl ₂	96.8	-0.20	97.4	94.6	118
0.1 M Mg(HMDS) ₂ /DME + 30 mM TBABH ₄	74.0	-0.40	99.9	98.6	119
0.1 M Mg(HMDS) ₂ /DME + 30 mM TBABH ₄ + 20 mM MgCl ₂	94.2	-0.25	99.7	98.9	226

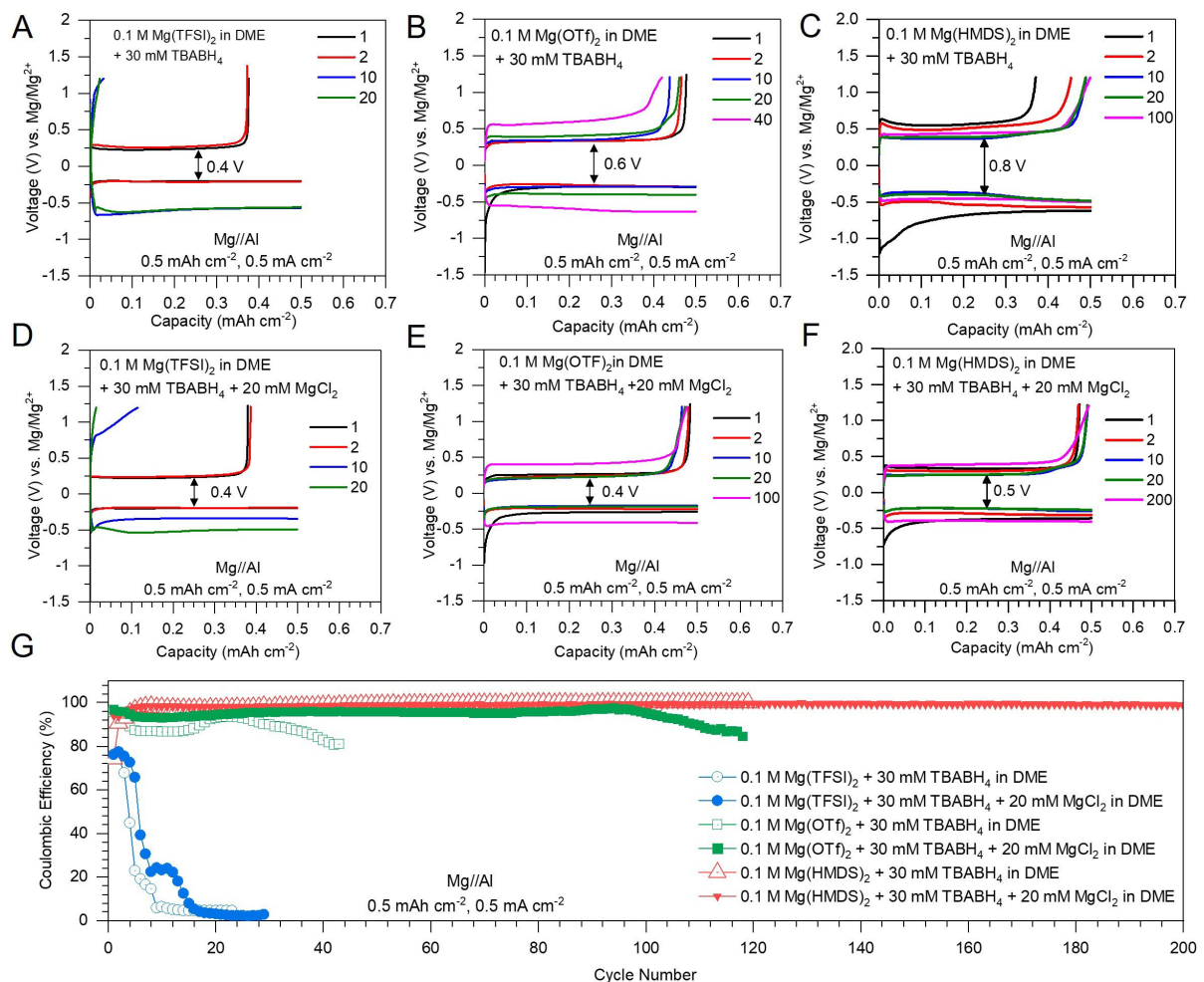


Figure 2. Plating and stripping profiles of Mg(TFSI)₂-based electrolytes A) without and D) with 20 mM MgCl₂, Mg(OTf)₂-based electrolytes B) without and E) with 20 mM MgCl₂, Mg(HMDS)₂-based electrolytes C) without and F) with 20 mM MgCl₂; G) Coulombic efficiency of various conventional electrolytes with 30 mM TBABH₄ and 20 mM MgCl₂ additives.

systems. In contrast to other salts, the CE of magnesium plating and stripping in the Mg(HMDS)₂/DME + 30 mM TBABH₄ increases after several cycles to achieve its optimum CE. The electrolyte also produces the highest average CE of 98.6% and the longest cycle life of ~120 cycles (Table 1). Based on this direct comparison of four electrolyte systems, we can conclude the following: 1) The Mg(ClO₄)₂ is incompatible with the Mg metal anode. 2) The Mg(TFSI)₂ and Mg(OTf)₂ in DME demonstrates limited reversibility of Mg plating/stripping. 3) The Mg(HMDS)₂/DME based electrolyte is the only conventional electrolyte that enables excellent reversibility of Mg plating/stripping. 4) The removal of moisture is crucial to the evaluation performance of Mg conventional electrolytes. The passivation of Mg metal anode caused by moisture contamination could result in underrating the performance of conventional Mg salts. 5) We concluded the compatibility of conventional salts lies in the order: Mg(HMDS)₂>Mg(OTf)₂>Mg(TFSI)₂. It is worth noting that several key factors would affect the magnesium plating and stripping process, which are the activation energy related to the desolvation (or solvation) of Mg²⁺ during the magnesium plating or stripping process, the

resistance associated with migration of Mg²⁺ across the SEI and of electroactive species across the boundary layer of the electrolyte, as well as the stability of the electrolyte constituents.^[2b,5] Hence, the high overpotential of Mg plating and stripping in the Mg(HMDS)₂/DME + 30 mM TBABH₄ electrolyte may have been due to several possible factors such as high desolvation energy of the Mg(HMDS)₂(DME) complex, or slow transport kinetics of Mg²⁺ in the electrolyte due to the formation of bulky complex in the electrolyte.

A recent study from Connell et al. showed that the reversibility of Mg anode is improved via controlled surface passivation by the formation of adsorbed Cl⁻ and/or MgCl₂ on the surface.^[13b] In this study, we introduced MgCl₂ at low concentration (~20 mM, ~0.21%wt) to each electrolyte. Performance enhancement with addition of MgCl₂ additive was observed in all three electrolyte solutions, including Mg(HMDS)₂, Mg(OTf)₂, and Mg(TFSI)₂ in DME + 30 mM TBABH₄. Firstly, the initial plating and stripping overpotential of magnesium reduces after the addition of MgCl₂. This effect is most prominent with the Mg(HMDS)₂ electrolyte (Figure 2F, Table 1), while it is less noticeable in the Mg(OTf)₂ (Figure 2E,

Table 1) and $\text{Mg}(\text{TFSI})_2$ (Figure 2D, Table 1) electrolytes. Secondly, the average CE of the magnesium plating and stripping process also improves upon the addition of MgCl_2 in the electrolytes. Most noticeable is the significant increase in the average CE of $\text{Mg}(\text{OTf})_2/\text{DME} + 30 \text{ mM TBABH}_4$ electrolyte from 88.6% to 94.6% (Figure 2G). On the other hand, a small improvement in the average CE from 17.8% to 21.8% is observed in the $\text{Mg}(\text{TFSI})_2$ -based electrolyte. Third, the addition of MgCl_2 extends the cell cycle life. This effect is most prominent in the $\text{Mg}(\text{HMDS})_2$ -based electrolyte, which improves from ~120 to ~220 cycles. It is worth noting that the end of asymmetric cell test is when short-circuit occurred (Figure S4). A possible mechanism that lengthened the cell lifetime is that MgCl_2 lowers the plating overpotential (Figures S5, 2 C and F), which results in a better Mg deposition morphology. The surface film formation in the case of electrolyte without MgCl_2 is an incremental process. The thickening of surface film caused by continuous decomposition of electrolyte components leads to inhomogeneous magnesium deposition, that eventually results in a short-circuit event. Herein, we propose the roles of MgCl_2 are: 1) Even at low concentration, MgCl_2 modifies the electroactive species in the electrolyte that reduces the activation energy of the Mg^{2+} desolvation process. 2) Chloride anion inhibits passivation through the formation of adsorbed Cl^- ($\text{Mg}-\text{Cl(ad)}$) and/or MgCl_2 on the surface and through a dynamic competition with H_2O in the double layer.^[13b]

The cycle life of the cell using $\text{Mg}(\text{OTf})_2$ -based electrolyte also improves significantly from ~40 cycles to ~120 cycles (Figure 2G). It is worth noting that the deposition potential in the $\text{Mg}(\text{ClO}_4)_2$ -based electrolyte is as low as ~3.2 V vs. Mg/Mg^{2+} (Figure S3B), even after the addition of MgCl_2 into the electrolyte. Overall, the addition of MgCl_2 showed improved electrochemical performance of the conventional electrolytes, but the stability of Mg salts against reduction at Mg metal anode remains a key factor to the electrochemical performance.

Further characterization with electrochemical impedance spectroscopy (EIS) shows the effect of magnesium salt stability and chloride concentration on the impedance of the magnesium anode (Figure S6). Magnesium anode immersed in $\text{Mg}(\text{HMDS})_2$ and $\text{Mg}(\text{OTf})_2$ shows a smaller charge transfer resistance than that in $\text{Mg}(\text{TFSI})_2$ electrolyte. Furthermore, $\text{Mg}(\text{HMDS})_2$ electrolyte shows a conditioning behavior that reduces the charge transfer resistance with each cycle of magnesium plating and stripping, whereas that of $\text{Mg}(\text{OTf})_2$ based electrolyte increases upon cycling. These trends revalidate the stability of $\text{Mg}(\text{HMDS})_2$ -electrolyte which prevents the build-up of a passivation layer on the anode. The addition of chloride maintains a low charge transfer resistance in the $\text{Mg}(\text{OTf})_2$ -electrolyte. We note however that the charge transfer resistance in the $\text{Mg}(\text{TFSI})_2$ -electrolyte increases with the use of MgCl_2 in the electrolyte but is reduced with each cycle. Overall, with the addition of MgCl_2 additives, the compatibility of conventional salts remains in the same order: $\text{Mg}(\text{HMDS})_2 > \text{Mg}(\text{OTf})_2 > \text{Mg}(\text{TFSI})_2$.

Given that the $\text{Mg}(\text{HMDS})_2$ -based electrolyte seems most suitable, further investigation is conducted on the properties of

the electrolyte. The symmetric cell profile in Figure S5 further validates the reduction of magnesium plating and stripping overpotential in the electrolyte upon the addition of MgCl_2 . However, the cell overpotential in the $\text{Mg}(\text{HMDS})_2 + \text{MgCl}_2$ -based electrolyte eventually equalizes with that in the chloride-free $\text{Mg}(\text{HMDS})_2$ -based electrolyte after prolonged cycling, indicating that the benefit of the chloride-based additives is short-termed. Chloride species are hypothesized to reduce the magnesium plating and stripping overpotential by removing the passivating film on the anode, preventing electrolyte decomposition, or tuning electroactive magnesium species.^[8] The short-termed effect of MgCl_2 in the $\text{Mg}(\text{HMDS})_2$ electrolyte likely relates to the consumption of the active chloride species which facilitates the processes described above.

Mg deposition morphology and interface chemical composition

Figure 3(A–F) shows the SEM image of electrochemical Mg deposits from 0.1 M $\text{Mg}(\text{TFSI})_2$, $\text{Mg}(\text{OTf})_2$, and $\text{Mg}(\text{HMDS})_2$ in DME. The electrochemical deposition process is conducted using a current density of 0.5 mA cm^{-2} on carbon-coated aluminum foil for 1 hour (i.e., 0.5 mAh cm^{-2}). The $\text{Mg}(\text{TFSI})_2$ -based electrolyte produces globular magnesium deposits (Figure 3A and D) akin to previous reports under similar plating current density.^[25] On the other hand, $\text{Mg}(\text{OTf})_2$ -based electrolyte forms a porous magnesium deposit film (Figure 3B and E), which potentially would lead to electrical isolation and the formation of “dead” magnesium crystals. This result explains the low CE of magnesium plating and stripping in this electrolyte. Crucially, the $\text{Mg}(\text{OTf})_2$ -based electrolyte was found to induce dendritic magnesium growth (shown in Figure S7) during the deposition process. In the asymmetric cell, the short-circuit can be detected by the rapid drop of voltage to near 0 V as marked in Figure S8. The magnesium deposits produced by the $\text{Mg}(\text{HMDS})_2$ -based electrolyte (Figure 3C and F) are well-defined crystals with uniform size and distribution.

The addition of MgCl_2 into the $\text{Mg}(\text{TFSI})_2$ -based electrolyte does not change the magnesium deposit morphology except for improving the magnesium globules distribution (Figure 3G and J). This result is consistent with negligible performance enhancement in the addition of MgCl_2 into $\text{Mg}(\text{TFSI})_2$ electrolyte. In the $\text{Mg}(\text{OTf})_2$ -based electrolyte, the addition of MgCl_2 reduces the porosity of the magnesium deposit film (Figure 3H and K), and crucially suppresses the dendrite formation in $\text{Mg}(\text{OTf})_2$ -based electrolyte. This result supports the extension of the cycle life of asymmetric cells using $\text{Mg}(\text{OTf})_2$ -based electrolyte with MgCl_2 additive. The morphology of the magnesium metal seems unchanged by the addition of MgCl_2 into the $\text{Mg}(\text{HMDS})_2$ -based (Figure 3I and L). Overall, the difference in the deposition morphology in each electrolyte may arise from various factors such as the diffusivity of ions during the deposition process, the deposition kinetics, the structure of the anode-electrolyte interface and may require further investigation to be established.^[4c,26]

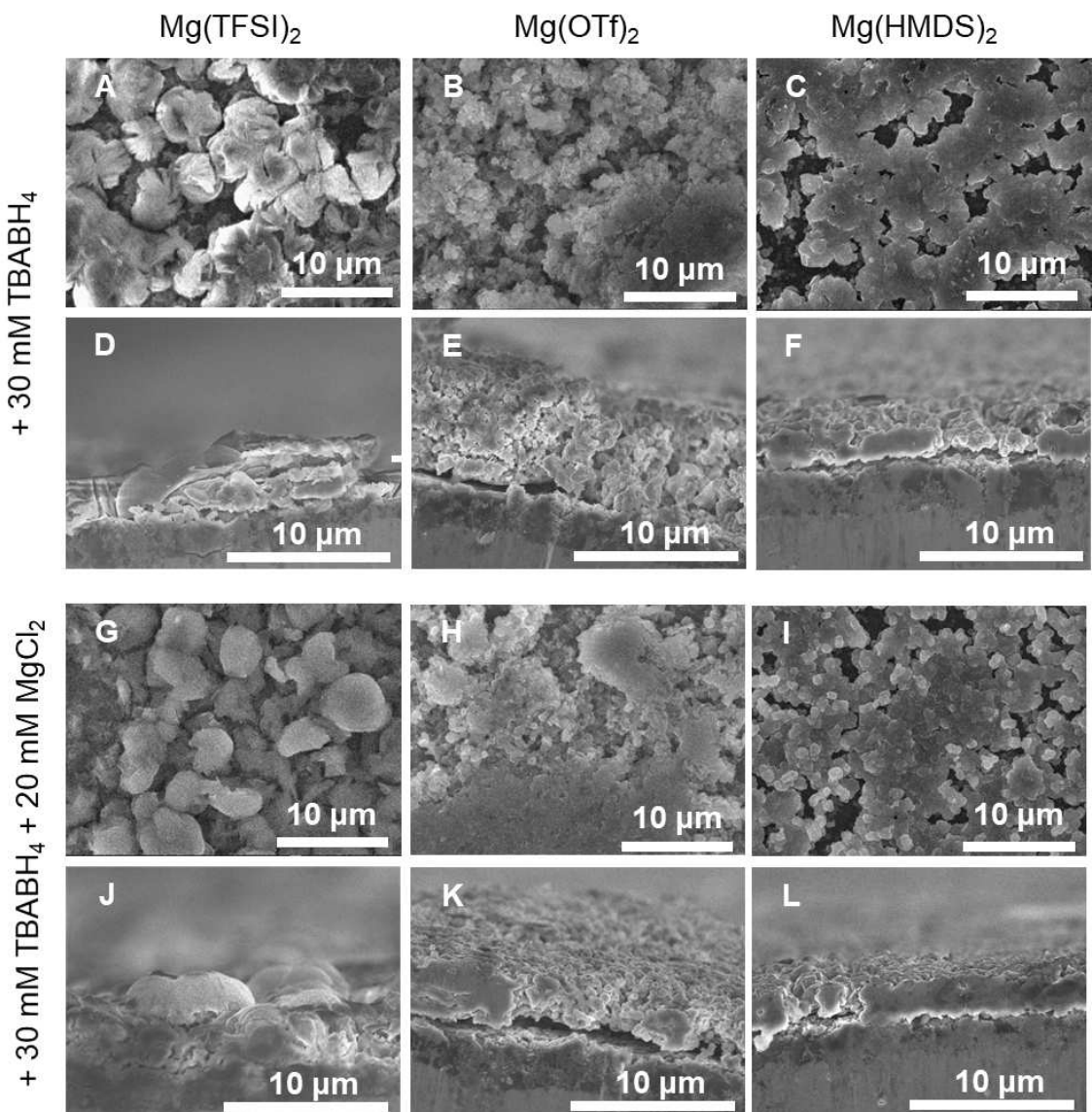


Figure 3. Magnesium deposit morphology from various conventional electrolytes. A and D) 0.1 M $\text{Mg}(\text{TFSI})_2$ + 30 mM TBABH_4 in DME. B and E) 0.1 M $\text{Mg}(\text{OTf})_2$ + 30 mM TBABH_4 in DME. C and F) 0.1 M $\text{Mg}(\text{HMDS})_2$ + 30 mM TBABH_4 in DME. G and J) 0.1 M $\text{Mg}(\text{TFSI})_2$ + 30 mM TBABH_4 + 20 mM MgCl_2 in DME. H and K) 0.1 M $\text{Mg}(\text{OTf})_2$ + 30 mM TBABH_4 + 20 mM MgCl_2 in DME. I and L) 0.1 M $\text{Mg}(\text{HMDS})_2$ + 30 mM TBABH_4 + 20 mM MgCl_2 in DME. Magnesium deposition process are conducted on carbon-coated aluminum electrode at 0.5 mA cm^{-2} and 0.5 mAh cm^{-2} .

Energy-dispersive X-ray spectroscopy (EDX) analysis further ascertains the composition of deposition film from electrolyte solutions (Figure 4). The concentration of Mg is in the order: $\text{Mg}(\text{TFSI})_2 < \text{Mg}(\text{OTf})_2 < \text{Mg}(\text{HMDS})_2$. Commonly observed impurities across all samples are C and O, indicating the decomposition of DME and anions. The deposits from $\text{Mg}(\text{TFSI})_2$ solution without MgCl_2 additive shows a high concentration of oxygen while carbon remained low, suggesting MgO and/or Mg(OH)_2 are likely the main components (Figure 4A). The reduction of OTf^- and TFSI^- against the magnesium metal is also evidenced by the existence of F and S elements in the $\text{Mg}(\text{OTf})_2$ - and $\text{Mg}(\text{TFSI})_2$ -derived samples (Figure 4A and B). The concentration of F and S is higher in the $\text{Mg}(\text{TFSI})_2$ -derived sample than that in the $\text{Mg}(\text{OTf})_2$ -derived sample, further proving that the OTf^- ion decomposition is less severe than

TFSI^- . Additional EDX analysis of the $\text{Mg}(\text{TFSI})_2$ -derived sample (Figure S9) also indicates that some deposit on the sample contains low magnesium concentration and high amount of C, O, F and S impurities, indicating that excessive parasitic reaction occurred in this electrolyte solution. This is well correlated to the low CE of Mg plating/stripping in $\text{Mg}(\text{TFSI})_2$ electrolytes. The inclusion of MgCl_2 into the electrolyte was also found to reduce the F and S concentration and increase the concentration of Mg in the $\text{Mg}(\text{OTf})_2$ and $\text{Mg}(\text{TFSI})_2$ -derived samples (Figure 4D and E). This result suggests that MgCl_2 prevents the decomposition of OTf^- and TFSI^- anions. In contrast, the deposited film from the $\text{Mg}(\text{HMDS})_2$ electrolyte demonstrates a high concentration of Mg (Figure 4C and F). We also note that the high concentration of carbon and aluminum in Figure 4F originated from carbon-coated aluminum foil

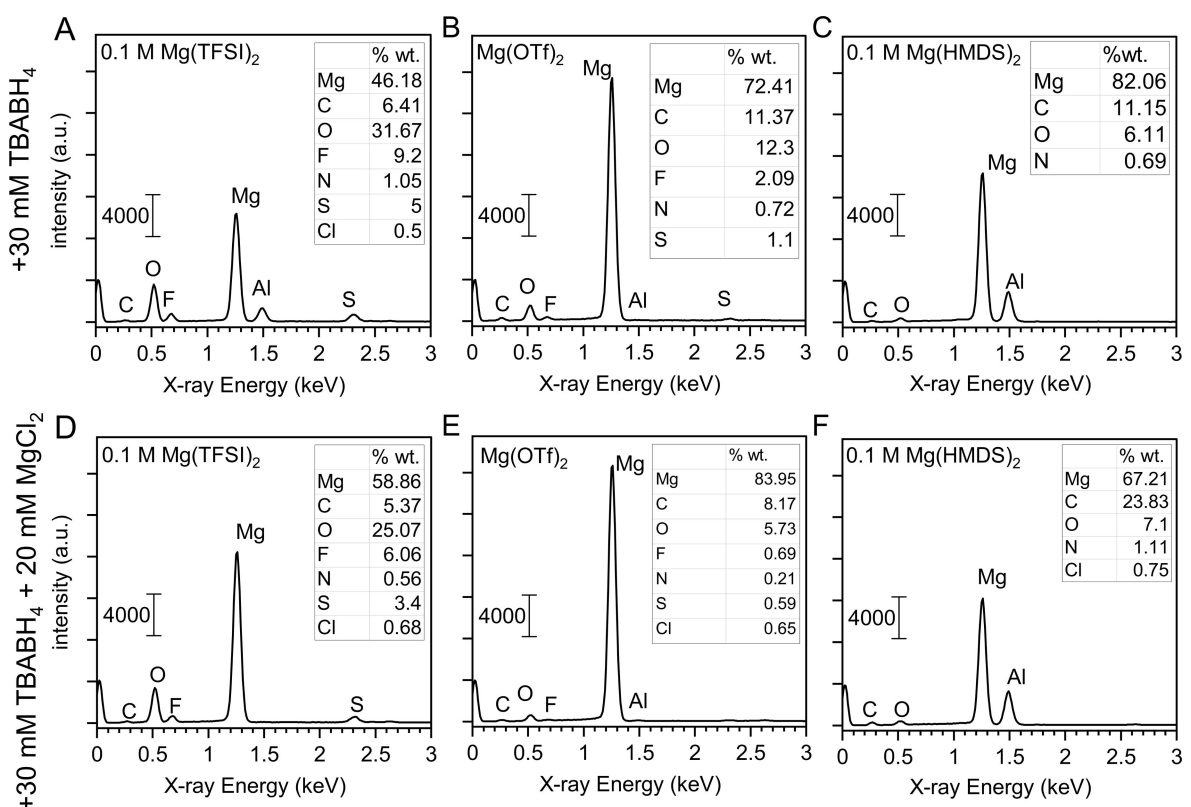


Figure 4. Elemental analysis of the magnesium deposits from each sample in Figure 3. EDX spectrum of deposits from electrolyte of A) $\text{Mg}(\text{TFSI})_2$, B) $\text{Mg}(\text{OTf})_2$, and C) $\text{Mg}(\text{HMDS})_2$ with TBABH_4 additive. EDX spectrum of deposits from D) $\text{Mg}(\text{TFSI})_2$, E) $\text{Mg}(\text{OTf})_2$, and F) $\text{Mg}(\text{HMDS})_2$ with TBABH_4 and MgCl_2 additives. The aluminum peak originated from the aluminum substrate. Elemental composition is rounded to two decimal places and the aluminum contribution from the current collector is excluded.

substrate, due to the thinner magnesium film formed from homogeneous deposition in the $\text{Mg}(\text{HMDS})_2$ electrolyte.

Figure 5 shows X-ray photoelectron spectroscopy (XPS) results of the Mg anode cycled in $\text{Mg}(\text{HMDS})_2$, $\text{Mg}(\text{OTf})_2$, and $\text{Mg}(\text{TFSI})_2$ electrolytes with TBABH_4 and $\text{TBABH}_4\text{-MgCl}_2$ additives. In general, the solid electrolyte interphase (SEI) components on Mg anode can be categorized into organic species which indicates DME decomposition,^[27] and inorganic species. Organic species can be identified from the C 1s spectrum where various organic functional groups are observed. These include C–O bonds (285.9 eV^[28]), C=O bonds (287.4 eV^[28b]), and C–C bonds (285 eV^[28b]). On the other hand, inorganic species can be identified from the spectra of other elements, these include MgO/MgF_2 , $\text{Mg}(\text{OH})_2$, and $\text{MgCO}_3/\text{MgCl}_2$ at 50.9 eV,^[28b,29] 51.5 eV,^[13b,29b,30] and 52.7 eV, respectively. The broad signal in low binding energy of Mg 2p spectra (49 eV) is assigned to Mg-dangling bond.^[31] The O 1s spectrum confirms the observation of MgO (529.1 eV^[28b]), $\text{Mg}(\text{OH})_2/\text{MgCO}_3$ (530.9 eV),^[29a,b,32] and C–O (532.6 eV^[28b]). It should be noted that the B 1s spectra in all samples show no clear signal of boron containing species, which is probably due to low concentration of TBABH_4 in electrolyte solutions (Figure S10A).

In $\text{Mg}(\text{HMDS})_2$ -based electrolyte, the C 1s spectra shows strong signal from C–O–C species (286 eV), which originated from reduction of DME.^[17] The C–O–C containing species is attributed to polyether and/or adsorbed-DME onto Mg surface.

A strong signal at 533 eV in O 1s spectra further supports the presence of polyether at Mg anode surface. This result suggests that the reduction of DME solvent plays an important role to the formation of the polymer-rich SEI in $\text{Mg}(\text{HMDS})_2$ -based electrolyte. The decomposition of HMDS⁻ anion is also confirmed by the presence of silicon carbide (Si–C) in C 1s spectra at 283.7 eV^[33] and supported by Si 2p spectra (Figure 6A). The C 1s, Mg 2p, and O 1s spectra of Mg anode cycled in $\text{Mg}(\text{HMDS})_2$ electrolyte without and with MgCl_2 show similar features and composition (Figure 6E). The presence of chloride on the surface of Mg anode is also confirmed (Figure 6B), suggesting the role of adsorbed-chloride additive in facilitating the Mg plating/stripping.

On Mg anode cycled in $\text{Mg}(\text{OTf})_2$ or $\text{Mg}(\text{TFSI})_2$ -based electrolyte, the C 1s spectra consist of various C=O containing species at 287.3 eV (C=O) and 288.9 eV (O=C=O–), which is most different from that in $\text{Mg}(\text{HMDS})_2$ system. The small signal at 293 eV is attributed to TFSI⁻ and OTf⁻ residual and –CF₂ species originated from decomposition of TFSI. In addition, the Mg 2p spectra in these electrolyte systems show a strong signal from MgO/MgF_2 , $\text{Mg}(\text{OH})_2$, and MgCO_3 . The decomposition of OTf⁻ and TFSI⁻ anion on the surface of Mg metal anode is evidenced by the strong signal of –SO₂ (531.9 eV) and O–F_x species (535 eV) in O 1s spectra (Figure 5), MgF₂ (685.5 eV) in F 1s spectra, and C–SO₂/SO₃²⁻ (168 eV), C–S–C (163.6 eV), sulfide (161.4 eV)^[28b] in S 2p spectra (Figure 6C and D). The formation

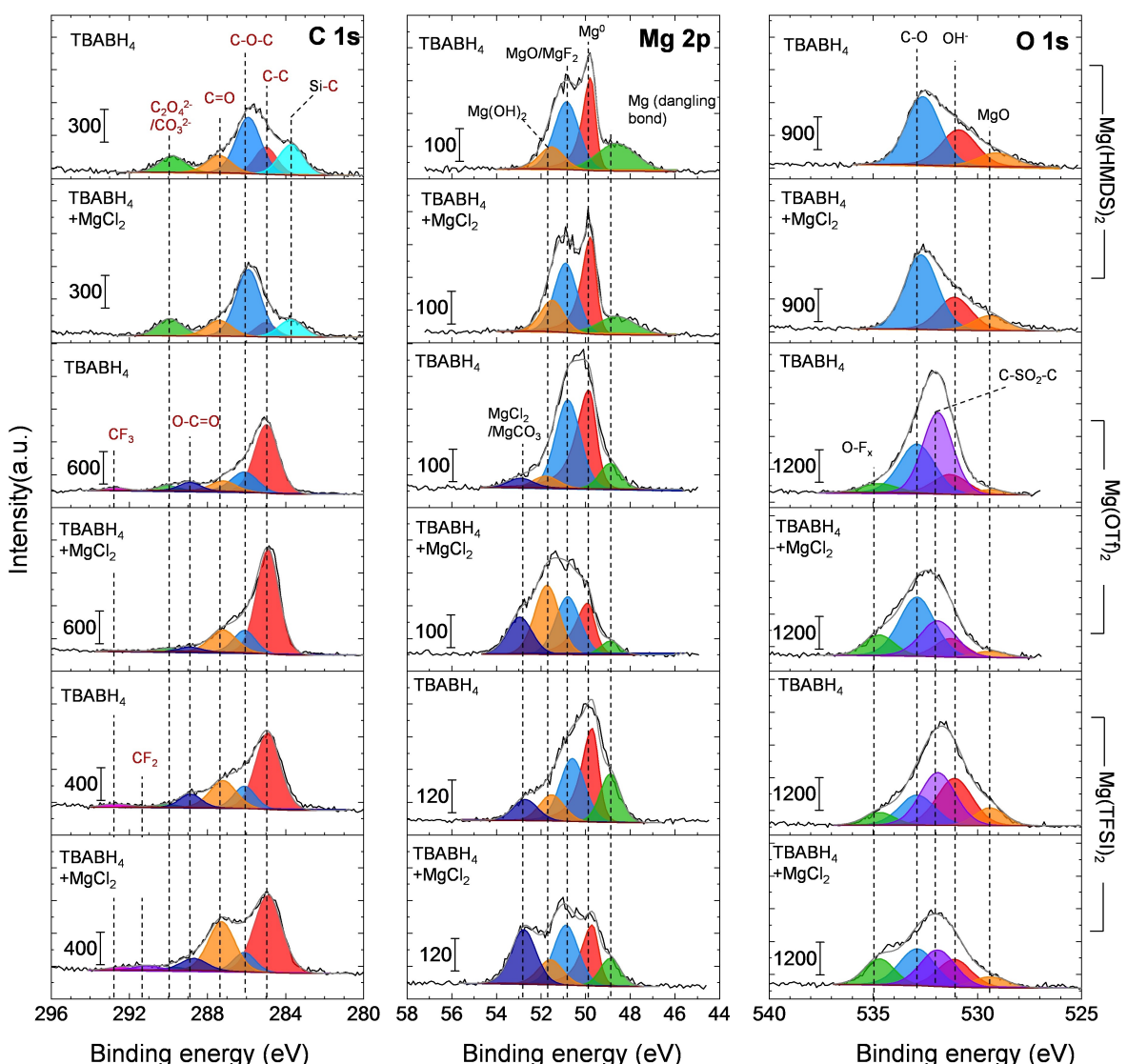


Figure 5. XPS analysis of magnesium electrodes after 20 cycles at 0.5 mA cm^{-2} and 0.5 mAh cm^{-2} . The electrolyte consists of 0.1 M Mg salts, Mg(HMDS)_2 , Mg(OTf)_2 , and Mg(TFSI)_2 in DME with 30 mM TBABH_4 and 30 mM $\text{TBABH}_4 + 20 \text{ mM}$ MgCl_2 additives.

of MgF_2 , SO_3^{2-} , $\text{C}-\text{S}-\text{C}$, and sulfide are important indications for the decomposition of OTf^- and TFSI^- anion, which mainly contribute to the formation of SEI in these electrolytes. In the presence of chloride additives, these signals show reduced intensities in Mg anode cycled in Mg(OTf)_2 electrolyte (Figure 6C and D). This result is consistent with the improved electrochemical performance with addition of chloride additive (Figure 2G). This suggests that the role of MgCl_2 additive (Figure S10B and C) is to reduce the decomposition of OTf^- anion. On the contrary, the addition of chloride additive shows negligible impact on preventing the decomposition of TFSI^- anion (Figure 6C-D). The concentration of MgF_2 , SO_3^{2-} , $\text{C}-\text{S}-\text{C}$, and sulfide species remains similar with and without MgCl_2 . This result is consistent with negligible performance enhancement in the electrochemical performance of Mg(TFSI)_2 with and without additives.

Based on the XPS analysis of the Mg interphase, we propose the structure of the active and passivated anodes

along with the effect of MgCl_2 on the SEI composition of the passivated anode. Mg(HMDS)_2 electrolyte produces a conducive SEI due to its thin organic polyether layer. On the other hand, the easily decomposed OTf^- and TFSI^- anions produce multiple inorganic species which adds to the thickness of the inorganic layer. This phenomenon causes a significant hindrance for Mg^{2+} ion migration across the SEI, since inorganic species like MgS , MgO , and MgF_2 are ionically insulating. The addition of a minuscule amount of MgCl_2 into Mg(OTf)_2 and Mg(TFSI)_2 electrolyte inhibits the decomposition of OTf^- and TFSI^- at the anode surface and, therefore, decreases the thickness of the passivating inorganic layer. However, the severe decomposition of TFSI^- results in poor electrochemical performance, which corresponds to negligible change in surface composition with and without MgCl_2 additive.

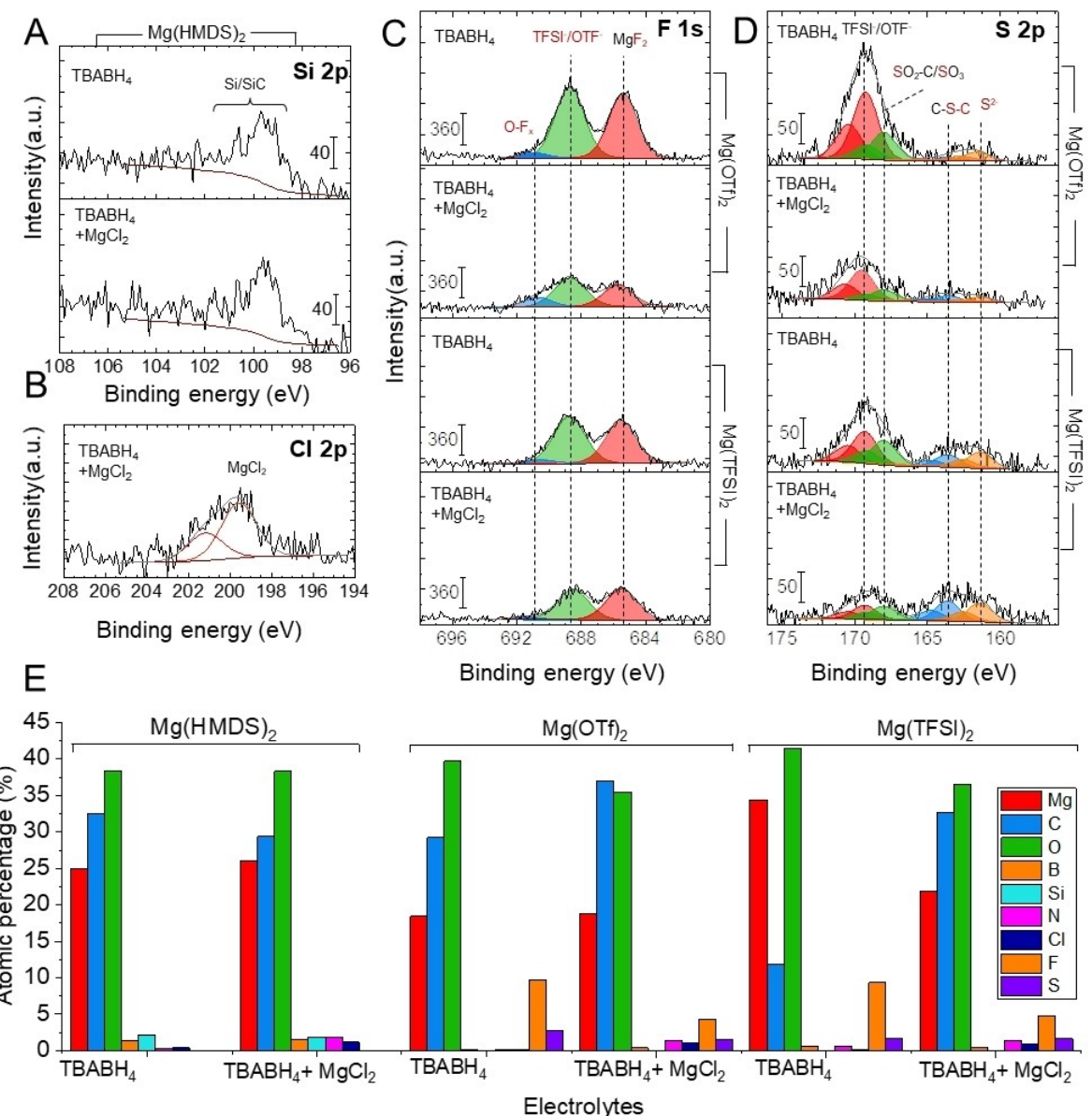


Figure 6. XPS analysis of magnesium electrodes after 20 cycles at 0.5 mA cm^{-2} and 0.5 mAh cm^{-2} . A) Si 2p and B) Cl 2p spectra of Mg anode cycled in Mg(HMDS)₂ with additives. C) F 1s and D) S 2p spectra of Mg anode cycled in Mg(OTf)₂ and Mg(TFSI)₂-based electrolyte with additives. E) Concentration (in atomic %) of Mg, C, O, B, Si, N, Cl, F and S elements on Mg anode cycled in Mg(HMDS)₂, Mg(OTf)₂, and Mg(TFSI)₂ electrolyte with additives.

Evidence of corrosion upon the addition of chloride salt

Chloride-based species is reported to cause current collector deterioration as it facilitates pitting metal corrosion.^[34] Hence the chloride content used in this study is minimized to millimolar concentration. Figure S11(A) shows the effect of adding MgCl₂ (~20 mM, ~0.21 wt.%) in the high-performance Mg(HMDS)₂-based electrolyte. Against stainless steel electrodes, the chloride-based electrolyte has a negligible anodic current when the electrode potential is below 2.24 V vs. Mg/Mg²⁺. Above 2.24 V, the anodic current rises dramatically compared to the control sample which does not contain MgCl₂. An increase in the anodic current at 1.5 V vs. Mg/Mg²⁺ due to the MgCl₂ was also observed on the Al working electrode. The

onset of anodic current around this potential is consistent with previous findings on the anodic stability of chloride-containing magnesium electrolytes on stainless steel and aluminium electrodes.^[6b,9a,c,35]

To further optimize the anodic stability of the 0.1 M Mg(HMDS)₂ electrolyte, the TBABH₄ concentration in the electrolyte is reduced from 30 mM to 20 mM due to ease of oxidation of BH₄⁻. As seen in Figures S11(B and C), reducing the TBABH₄ concentration significantly reduces the anodic decomposition current on the stainless steel electrode at high potential. We further highlight the need to eliminate chloride from the electrolyte solution as it initiates corrosion even at extremely low concentrations (~5 mM MgCl₂, ~0.05 wt.%). Based on the linear sweep voltammetry (LSV) measurement in

Figure 7(A), the chloride-free electrolyte (control) has anodic stability of 2.59 V on aluminium and 3.09 V on stainless steel. The small inclusion of $MgCl_2$ into the electrolyte does not show a significant reduction in the anodic stability of the electrolyte against stainless steel electrodes (Figure S12A). However, a more accurate anodic stability measurement using chronoamperometry shows a contradictory result. Figure S12(B and C) shows the anodic current on the stainless steel electrode rises significantly at 2.625 V vs. Mg/Mg^{2+} upon the addition of chloride into the electrolyte. Furthermore, extended chronoamperometry measurements for 3 hours on the stainless steel electrode seems to show that the corrosion current could significantly rise to $\sim 0.2 \text{ mA cm}^{-2}$ (Figure S12D), which is typical behaviour of corrosion process. Similarly, Al electrode shows

small current ($< 10 \mu\text{A}$) during chronoamperometry measurements up to 2.8 V. However, addition of 20 mM of $MgCl_2$ show current rising during chronoamperometry measurements at 2.8 V, indicating the corrosion of Al caused by the present of chloride salt (Figure S12E).

To confirm the corrosion behaviour of $Mg(HMDS)_2$ electrolyte with and without 20 mM $MgCl_2$, the surfaces of the stainless steel and aluminium electrodes are analysed after the measurement. Figure S13(A) shows the surface of the stainless steel electrode after it is held at 2.625 V vs. Mg/Mg^{2+} in the chloride-containing electrolyte for 3 hours, which clearly shows the existence of a corrosion pit, thereby affirming that the high current density in Figure S12(D) is due to corrosion. Similarly, Figure S13(B) also shows the existence of aluminium corrosion

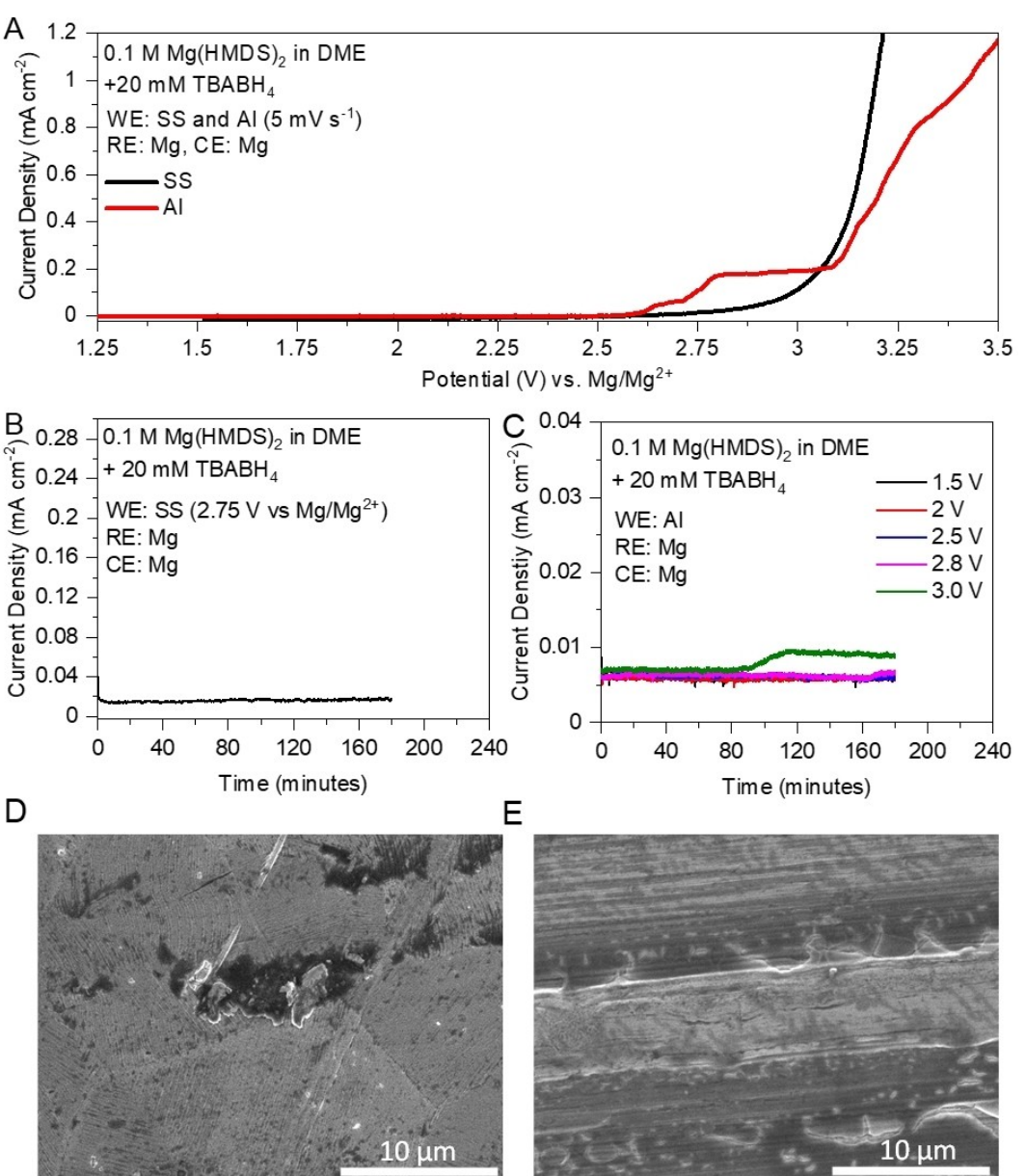


Figure 7. A) LSV measurement of chloride-free $Mg(HMDS)_2$ -based electrolyte on stainless steel and aluminium electrodes. B and C) Chronoamperometry of B) stainless steel electrode and C) aluminium electrode in 0.1 M $Mg(HMDS)_2$ + 20 mM $TBABH_4$ in DME. SEM of D) stainless steel and E) aluminium electrodes surface in 0.1 M $Mg(HMDS)_2$ + 20 mM $TBABH_4$ in DME.

pit after the chronoamperometry experiment in the chloride-containing electrolyte. On the other hand, the SEM analysis of the electrodes after the chronoamperometry measurement in Figure 7(D and E) indicates no observation of pitting corrosion in chloride-free electrolyte. The chronoamperometry measurements, therefore, show that a minuscule amount of chloride as low as 5 mM MgCl₂ induce corrosion on the stainless steel and aluminium electrodes. As shown in Figure S14(D), the plating and stripping overpotential of magnesium in the electrolyte is relatively unchanged with the addition of 5 mM of MgCl₂. Additional characterization in Figure S15(A) revalidates successful electrochemical deposition of magnesium in the Mg-(HMDS)₂-electrolyte and the development of densely packed magnesium crystal upon plating and stripping without the use of MgCl₂ additive. Hence, our result here proves that Mg-(HMDS)₂ can facilitate highly reversible Mg plating/stripping without the need for chloride containing additive.

Conclusion

Examination of four commercially available Mg salts under similar conditions show that only Mg(HMDS)₂ can enable highly reversible Mg plating/stripping. Mg(OTf)₂ and Mg(TFSI)₂ also demonstrate reversible Mg plating/stripping but passivation still occurs due to reduction of OTf⁻ and TFSI⁻ anion, while Mg anode shows complete passivation upon contact with Mg-(ClO₄)₂-based electrolyte. The electrochemical performance of conventional electrolyte salts hence lies in the order: Mg-(HMDS)₂ (highly reversible) > Mg(OTf)₂ (partially reversible) > Mg(TFSI)₂ (severe decomposition) > Mg(ClO₄)₂ (complete passivation). Through the evaluation of electrochemical performance with TBABH₄, we also highlight the need to alleviate the passivating effect of water impurity in the electrolyte to accurately infer the stability of each electrolyte salt, especially in a chloride-free electrolyte system.

Surface analysis of Mg anode after cycling shows that decomposition of anions such as TFSI⁻ and OTf⁻ form a thicker inorganic layer along with ionically insulating constituents such as MgS, MgO, and MgF₂. To improve the electrochemical performance of these electrolytes, the use of MgCl₂ is needed to facilitate the reversibility of Mg plating/stripping process, especially in Mg(OTf)₂-based electrolyte. However, the use of MgCl₂ additive as low as 5 mM comes with compromise of anodic stability due to corrosion of current collectors such as stainless steel and aluminium. In contrast, the stable Mg-(HMDS)₂ salt minimizes the formation of MgO on the interphase and forms a thin organic polyether layer on the anode, which allows for relatively uninhibited Mg²⁺ migration across the interphase. As a result, Mg(HMDS)₂ electrolyte can deliver reversible Mg plating/stripping without the need for MgCl₂ additive. Through this study, we provide a practical evaluation of commercially available Mg salts and a guide for the selection of electrolyte composition for future studies of high-energy-density rechargeable Mg batteries.

Author contributions

Conceptualization: R.H., D.-T.N. and Z.W.S.; Data collection, investigation and validation: R.H., D.-T.N. and A.Y.S.E.; writing - original draft: R.H. and D.-T.N.; writing – review and editing, Supervision: Z.W.S. All authors have given approval to the final version of the manuscript.

Acknowledgements

This work is supported by the Singapore National Research Foundation (NRF-NRFF2017-04) and Agency for Science, Technology and Research (Central Research Fund Award).

Conflict of Interest

There are no conflicts to declare.

Data Availability Statement

The data that support the findings of this study are available from the corresponding author upon reasonable request.

Keywords: chloride-free electrolyte • conventional electrolyte • passivation layer • rechargeable magnesium battery • solid electrolyte interphase

- [1] a) Z. P. Cano, D. Banham, S. Ye, A. Hintennach, J. Lu, M. Fowler, Z. Chen, *Nat. Energy* **2018**, *3*, 279–289; b) T. Chen, Y. Jin, H. Lv, A. Yang, M. Liu, B. Chen, Y. Xie, Q. Chen, *Trans. Tianjin Univ.* **2020**, *26*, 208–217; c) T. M. Gür, *Energy Environ. Sci.* **2018**, *11*, 2696–2767.
- [2] a) Y. Liang, H. Dong, D. Aurbach, Y. Yao, *Nat. Energy* **2020**, *5*, 646–656; b) M. Li, J. Lu, X. Ji, Y. Li, Y. Shao, Z. Chen, C. Zhong, K. Amine, *Nat. Rev. Mater.* **2020**, *5*, 276–294; c) R. Mohtadi, F. Mizuno, *Beilstein J. Nanotechnol.* **2014**, *5*, 1291–1311.
- [3] M. Weil, S. Zieman, J. Peters, in *Behaviour of Lithium-Ion Batteries in Electric Vehicles: Battery Health, Performance, Safety, and Cost* (Eds.: G. Pistoia, B. Liaw), Springer International Publishing, Cham, **2018**, pp. 59–74.
- [4] a) H. D. Yoo, I. Shterenberg, Y. Gofer, G. Gershinsky, N. Pour, D. Aurbach, *Energy Environ. Sci.* **2013**, *6*, 2265–2279; b) F. Liu, T. Wang, X. Liu, L. Z. Fan, *Adv. Energy Mater.* **2020**, *11*, 2000787; c) F. Hao, A. Verma, P. P. Mukherjee, *Energy Storage Mater.* **2019**, *20*, 1–6; d) C. Ling, D. Banerjee, M. Matsui, *Electrochim. Acta* **2012**, *76*, 270–274.
- [5] P. Bonnick, J. Muldoon, *Adv. Funct. Mater.* **2020**, *30*, 1910510.
- [6] a) P. Canepa, G. Sai Gautam, D. C. Hannah, R. Malik, M. Liu, K. G. Gallagher, K. A. Persson, G. Ceder, *Chem. Rev.* **2017**, *117*, 4287–4341; b) Y. Yang, Y. Qiu, Y. NuLi, W. Wang, J. Yang, J. Wang, *J. Mater. Chem. A* **2019**, *7*, 18295–18303.
- [7] a) C. B. Bucur, T. Gregory, A. G. Oliver, J. Muldoon, *J. Phys. Chem. Lett.* **2015**, *6*, 3578–3591; b) J. Song, E. Sahadeo, M. Noked, S. B. Lee, *J. Phys. Chem. Lett.* **2016**, *7*, 1736–1749; c) R. Attias, M. Salama, B. Hirsch, Y. Goffer, D. Aurbach, *Joule* **2019**, *3*, 27–52.
- [8] X. Zhao, Z. Zhao-Karger, M. Fichtner, X. Shen, *Angew. Chem. Int. Ed.* **2020**, *59*, 5902–5949; *Angew. Chem.* **2020**, *132*, 5954–6004.
- [9] a) D. Huang, S. Tan, M. Li, D. Wang, C. Han, Q. An, L. Mai, *ACS Appl. Mater. Interfaces* **2020**, *12*, 17474–17480; b) T. Gao, S. Hou, F. Wang, Z. Ma, X. Li, K. Xu, C. Wang, *Angew. Chem. Int. Ed.* **2017**, *56*, 13526–13530; *Angew. Chem.* **2017**, *129*, 13711–13715; c) J. Luo, S. He, T. L. Liu, *ACS Energy Lett.* **2017**, *2*, 1197–1202.

- [10] a) Z. Zhao-Karger, M. E. Gil Bardaji, O. Fuhr, M. Fichtner, *J. Mater. Chem. A* **2017**, *5*, 10815–10820; b) Z. Zhao-Karger, R. Liu, W. Dai, Z. Li, T. Diermant, B. P. Vinayan, C. Bonatto Minella, X. Yu, A. Manthiram, R. J. Behm, M. Ruben, M. Fichtner, *ACS Energy Lett.* **2018**, *3*, 2005–2013.
- [11] a) T. Mandai, *ACS Appl. Mater. Interfaces* **2020**, *12*, 39135–39144; b) K. Tang, A. Du, S. Dong, Z. Cui, X. Liu, C. Lu, J. Zhao, X. Zhou, G. Cui, *Adv. Mater.* **2020**, *32*, 1904987.
- [12] a) X. Li, T. Gao, F. Han, Z. Ma, X. Fan, S. Hou, N. Eidson, W. Li, C. Wang, *Adv. Energy Mater.* **2018**, *8*, 1701728; b) J. Zhang, X. Guan, R. Lv, D. Wang, P. Liu, J. Luo, *Energy Storage Mater.* **2020**, *26*, 408–413; c) R. Lv, X. Guan, J. Zhang, Y. Xia, J. Luo, *Natl. Sci. Rev.* **2019**, *7*, 333–341.
- [13] a) H. Wang, X. Feng, Y. Chen, Y.-S. Liu, K. S. Han, M. Zhou, M. H. Engelhard, V. Murugesan, R. S. Assary, T. L. Liu, W. Henderson, Z. Nie, M. Gu, J. Xiao, C. Wang, K. Persson, D. Mei, J.-G. Zhang, K. T. Mueller, J. Guo, K. Zavadil, Y. Shao, J. Liu, *ACS Energy Lett.* **2020**, *5*, 200–206; b) J. G. Connell, B. Genorio, P. P. Lopes, D. Strmcnik, V. R. Stamenkovic, N. M. Markovic, *Chem. Mater.* **2016**, *28*, 8268–8277.
- [14] J. Muldoon, C. B. Bucur, A. G. Oliver, J. Zajicek, G. D. Allred, W. C. Boggess, *Energy Environ. Sci.* **2013**, *6*, 482–487.
- [15] S. Hou, X. Ji, K. Gaskell, P.-f. Wang, L. Wang, J. Xu, R. Sun, O. Borodin, C. Wang, *Science* **2021**, *374*, 172–178.
- [16] A. L. Lipson, S.-D. Han, B. Pan, K. A. See, A. A. Gewirth, C. Liao, J. T. Vaughey, B. J. Ingram, *J. Electrochem. Soc.* **2016**, *163*, A2253–A2257.
- [17] R. Horia, D.-T. Nguyen, A. Y. S. Eng, Z. W. Seh, *Nano Lett.* **2021**, *21*, 8220–8228.
- [18] M. Salama, I. Shterenberg, H. Gizbar, N. N. Eliaz, M. Kosa, K. Keinan-Adamsky, M. Afri, L. J. W. Shimon, H. E. Gottlieb, D. T. Major, Y. Gofer, D. Aurbach, *J. Phys. Chem. C* **2016**, *120*, 19586–19594.
- [19] P. Schüler, H. Görls, M. Westerhausen, S. Krieck, *Dalton Trans.* **2019**, *48*, 8966–8975.
- [20] I. Shterenberg, M. Salama, H. D. Yoo, Y. Gofer, J.-B. Park, Y.-K. Sun, D. Aurbach, *J. Electrochem. Soc.* **2015**, *162*, A7118–A7128.
- [21] E. Klindtworth, I. Delidovich, R. Palkovits, *Int. J. Hydrogen Energy* **2018**, *43*, 20772–20782.
- [22] Y. Gofer, O. Chusid, H. Gizbar, Y. Viestfrid, H. E. Gottlieb, V. Marks, D. Aurbach, *Electrochem. Solid-State Lett.* **2006**, *9*, A257.
- [23] M. Salama, I. Shterenberg, L. J. W. Shimon, K. Keinan-Adamsky, M. Afri, Y. Gofer, D. Aurbach, *J. Phys. Chem. C* **2017**, *121*, 24909–24918.
- [24] Y. Chen, N. R. Jaegers, H. Wang, K. S. Han, J. Z. Hu, K. T. Mueller, V. Murugesan, *J. Phys. Chem. Lett.* **2020**, *11*, 6443–6449.
- [25] a) J. Eaves-Rather, K. Moyer, M. Zohair, C. L. Pint, *Joule* **2020**, *4*, 1324–1336; b) M. S. Ding, T. Diermant, R. J. Behm, S. Passerini, G. A. Giffin, *J. Electrochem. Soc.* **2018**, *165*, A1983–A1990.
- [26] a) L. Guo, P. C. Searson, *Electrochim. Acta* **2010**, *55*, 4086–4091; b) R. Davidson, A. Verma, D. Santos, F. Hao, C. D. Fincher, D. Zhao, V. Attari, P. Schofield, J. Van Buskirk, A. Fraticelli-Cartagena, T. E. G. Alivio, R. Arroyave, K. Xie, M. Pharr, P. P. Mukherjee, S. Banerjee, *Mater. Horiz.* **2020**, *7*, 843–854.
- [27] a) V. Kumar, A. Y. S. Eng, Y. Wang, D.-T. Nguyen, M.-F. Ng, Z. W. Seh, *Energy Storage Mater.* **2020**, *29*, 1–8; b) M. Arsentev, A. Missyul, A. V. Petrov, M. Hammouri, *J. Phys. Chem. C* **2017**, *121*, 15509–15515.
- [28] a) D. Briggs, *Surf. Interface Anal.* **1981**, *3*, v–v; b) A. V. Naumkin, A. Kraut-Vass, S. W. Gaarenstroom, C. J. Powell, *Vol.* **2021**, National Institute of Standards and Technology, **2012**.
- [29] a) P. J. Burke, Z. Bayindir, G. J. Kipouros, *Appl. Spectrosc.* **2012**, *66*, 510–518; b) B. V. Christ, *Handbook of Monochromatic XPS Spectra: The Elements and Native Oxides*, Vol. 1, XPS International, Salem (OR), **1999**; c) H. Kuwata, M. Matsui, N. Imanishi, *J. Electrochem. Soc.* **2017**, *164*, A3229–A3236.
- [30] a) T. Gao, S. Hou, K. Huynh, F. Wang, N. Eidson, X. Fan, F. Han, C. Luo, M. Mao, X. Li, C. Wang, *ACS Appl. Mater. Interfaces* **2018**, *10*, 14767–14776; b) D.-T. Nguyen, A. Y. S. Eng, M.-F. Ng, V. Kumar, Z. Sofer, A. D. Handoko, G. S. Subramanian, Z. W. Seh, *Cell Rep. Phys. Sci.* **2020**, *1*, 100265; c) D.-T. Nguyen, A. Y. S. Eng, R. Horia, Z. Sofer, A. D. Handoko, M.-F. Ng, Z. W. Seh, *Energy Storage Mater.* **2022**, *45*, 1120–1132.
- [31] N. Kamarulzaman, N. F. Chayed, N. Badar, M. F. Kasim, D. T. Mustaffa, K. Elong, R. Rusdi, T. Oikawa, H. Furukawa, *ECS J. Solid State Sci. Technol.* **2016**, *5*, Q3038–Q3045.
- [32] a) X. D. Peng, M. A. Bartea, *Surf. Sci.* **1990**, *233*, 283–292; b) H. B. Yao, Y. Li, A. T. S. Wee, *Appl. Surf. Sci.* **2000**, *158*, 112–119; c) P. Casey, G. Hughes, E. O'Connor, R. D. Long, P. K. Hurley, *J. Phys. Conf. Ser.* **2008**, *100*, 042046.
- [33] G. Beamson, *The Scienta ESCA 300 Database* **1992**.
- [34] a) G. S. Frankel, *J. Electrochem. Soc.* **1998**, *145*, 2186–2198; b) J. Soltis, *Corros. Sci.* **2015**, *90*, 5–22.
- [35] a) Z. Zhao-Karger, X. Zhao, O. Fuhr, M. Fichtner, *RSC Adv.* **2013**, *3*, 16330–16335; b) A. Du, Z. Zhang, H. Qu, Z. Cui, L. Qiao, L. Wang, J. Chai, T. Lu, S. Dong, T. Dong, H. Xu, X. Zhou, G. Cui, *Energy Environ. Sci.* **2017**, *10*, 2616–2625.

Manuscript received: January 4, 2022

Revised manuscript received: February 22, 2022

Accepted manuscript online: February 23, 2022